THE JOURNAL OF PHYSICAL CHEMISTRY C

Article

pubs.acs.org/JPCC

Rendering High Charge Density of States in Ionic Liquid-Gated MoS_2 Transistors

Yeonsung Lee,[†] Jiyoul Lee,[‡] Sunkook Kim,*[,†] and Ho Seok Park*[,§]

[†]Multi-Functional Nano/Bio Electronics Lab., Department of Electronics and Radio Engineering, Kyung Hee University, Gyeonggi 446-701, South Korea

[‡]Holst Centre/TNO, High Tech Campus #31, Eindhoven 5656AE, The Netherlands

[§]School of Chemical Engineering, Sungkyunkwan University (SKKU), Suwon 440-746, Republic of Korea

ABSTRACT: We investigated high charge density of states (DOS) in the bandgap of MoS_2 nanosheets with variable temperature measurements on ionic liquid-gated MoS_2 transistors. The thermally activated charge transport indicates that the electrical current in the two-dimensional MoS_2 nanosheets under high charge density state follows the Meyer-Neldel rule. The achieved high charge density allows the surface DOS estimation of MoS_2 nanosheets, which have distinct peaks at 0.135 and 0.145 eV below the conduction band, with the largest DOS values of 9.75×10^{14} and 4.33×10^{14} cm^{-2} eV^{-1}, respectively. This may represent the monolayer MoS_2 nanosheets that coexist with the MoS_2 multilayer in the channel area of the ionic liquid-gated MoS_2 transistors.

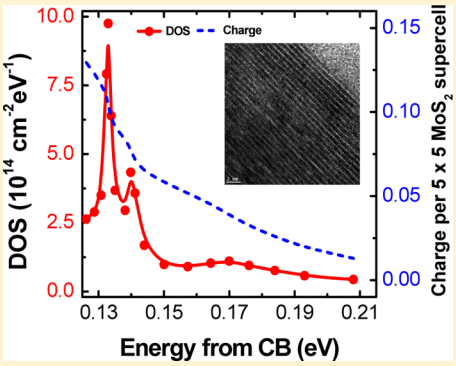

1. INTRODUCTION

Since the discovery of graphene in 2004, two-dimensional (2D) nanosheet materials have been widely explored as promising candidates for postsilicon semiconducting materials due to their potential for future electronic applications, such as high speed semiconductor chips on flexible substrates and transparent optoelectronics applications.[1,2] In particular, the benchmark player of 2D materials, graphene, shows excellent intrinsic optoelectronic properties and mechanical compatibility with plastic substrates, which are desirable for flexible electronics. Although 2D graphene has these exciting optical and mechanical properties, the zero-band gap in its electronic structure (a very low on/off current ratio < 100) makes it unsuitable for a switching device in integrated circuitry.[2−5]

Alternately, the transition metal dichalcogenide molybdenum disulfide (MoS_2), consisting of a Mo atom layer sandwiched between two sulfurs, has attracted great interest because it has electronic properties that are comparable to those of graphene but with sizable band-gaps due to its asymmetry at the atomic level.[6,7] Motivated by the distinct electronic properties of MoS_2 materials, we previously presented process-friendly multilayer MoS_2 thin-film transistors with high mobility of >100 $cm^2/(V\,s)$ and robust current saturation over a large voltage window.[7] Very recently, Perera et al. also reported few-layer MoS_2-based transistors showing a high electron mobility of 60 $cm^2/(V\,s)$, a high on/off current ratio of 10,[7] and near-ideal subthreshold swings of ∼50 mV per decade with the help of electrolyte gating.[8] However, despite these intensive studies on the device's performance, the fundamental behaviors underlying the charge transport phenomena on the surface of the MoS_2 nanosheet remain controversial. This is mainly attributed to the lack of an experimentally proven study examining its electronic structures such as the density of states (DOS), which is essential to understand the intrinsic charge transporting characteristics.

In this article, we experimentally extracted the DOS in the MoS_2 nanosheet with electrostatic double layer (EDL)-gated transistors (EDLTs) from the experimental temperature-dependent current−voltage (IV) measurement, consisting of source and drain electrodes and an MoS_2 channel interfacing with a gate electrode in ionic contact using electrolytes. EDLTs using a highly capacitive EDL have significant advantages over conventional dielectric-based transistors in terms of the enhanced drain current, low operating voltages, new device configurations (e.g., coplanar gate structures), and the solution processability of solid electrolytes.[9,10] In particular, ionic liquids (ILs), which are composed of large organic cations and weakly coordinating anions, have received a great deal of attention as electrolytes due to their high ionic conductivity, wide electrochemical window, low vapor pressures, and chemical and physical stability.[11] Along with the nonvolatility and thermal stability, these characteristics allow ILs to reliably operate EDLTs at high temperatures (>100 °C) through a thermally activated ion transport.[10−13]

2. EXPERIMENTAL SECTION

Device Fabrication. The MoS_2 nanosheet-based EDLT devices were fabricated with source/drain electrodes, Ti(20

Received: June 26, 2014
Revised: July 16, 2014
Published: July 16, 2014

   dx.doi.org/10.1021/jp5063836 | J. Phys. Chem. C 2014, 118, 18278−18282

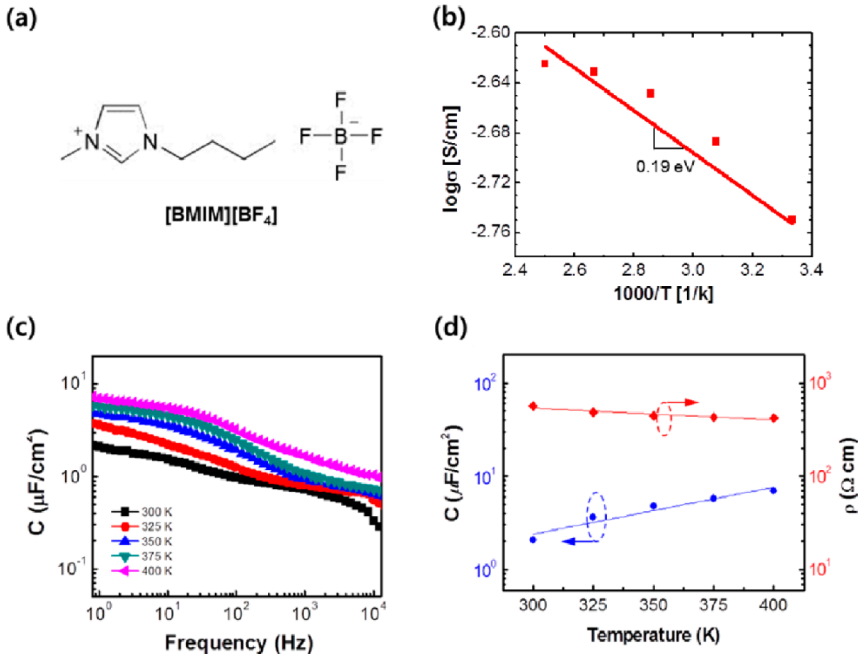

Figure 1. (a) Molecular structures of 1-butyl-3-methyl-imidazolium tetrafluoroborate ($BMimBF_4$) ionic liquids (ILs) used in this work. (b) Complex plane of the $BMimBF_4$ ILs measured from the impedance spectroscopy, (c) capacitance vs. frequency plot, and (d) summarized plot of the temperature-dependent capacitance and resistivity of the $BMimBF_4$ ILs.

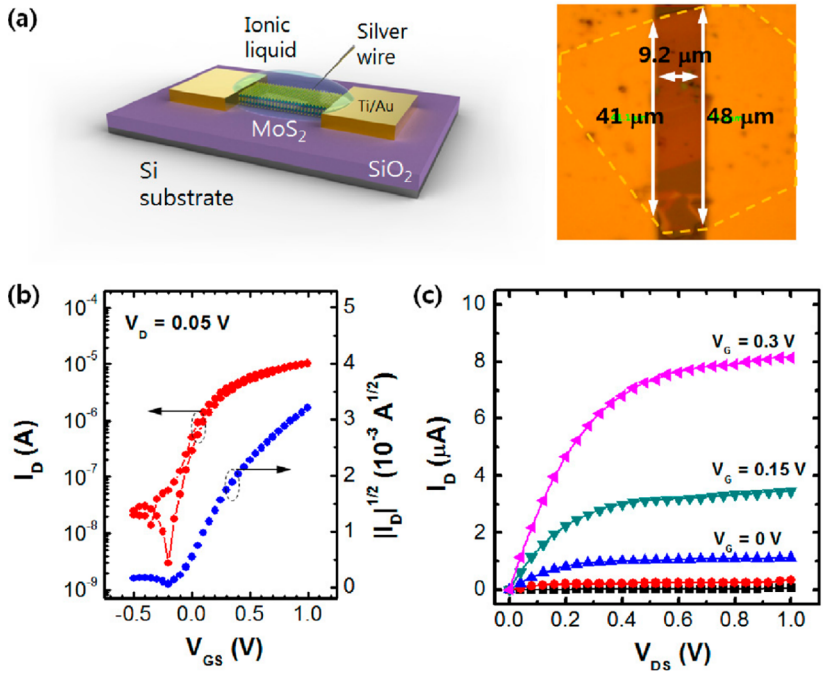

Figure 2. A MoS_2 nanosheet-based EDLT with IL gating on a SiO_2/Si substrate and its electrical characteristics. (a) Schematic depiction and optical photographic image of the device. (b) The linear scale and log scale I_d–V_{gs} characteristics and (c) output curves from the MoS_2 EDLT.

nm)/Au(300 nm), which were deposited by an electron beam evaporator. Thin flakes of MoS_2 were mechanically exfoliated from bulk MoS_2 crystals using Scotch tape and were then deposited on an SiO_2 (300 nm) dielectric and Si substrate as reported in our previous work.[7] Large-scaled stripes of Ti/Au electrodes (0.2 × 1.5 cm) are patterned by using standard photolithography, which makes it easy to align the PDMS structure on the channel for the IL droplets. 1-Butyl-3-methylimidazolium tetrafluoroborate ($BMimBF_4$) was used as dielectric ILs. $BMimBF_4$ ILs with sizes of ~50 μL are dropped onto the channel in the rectangular form of the PDMS to prevent the leakage of liquid electrolytes between the MoS_2 channel and the source/drain electrodes. For the electrolyte gating, silver wire was directly immersed in the IL gate medium and served as the top gate. The channel dimensions estimated by an optical microscope included a length of 41.1 μm and a width of 9.2 μm.

Characterization. The ionic conductivity and capacitance of ILs was measured by the AC impedance spectroscopy (a Solatron 1255 frequency response analyzer) over a frequency

dx.doi.org/10.1021/jp5063836 | J. Phys. Chem. C 2014, 118, 18278–18282

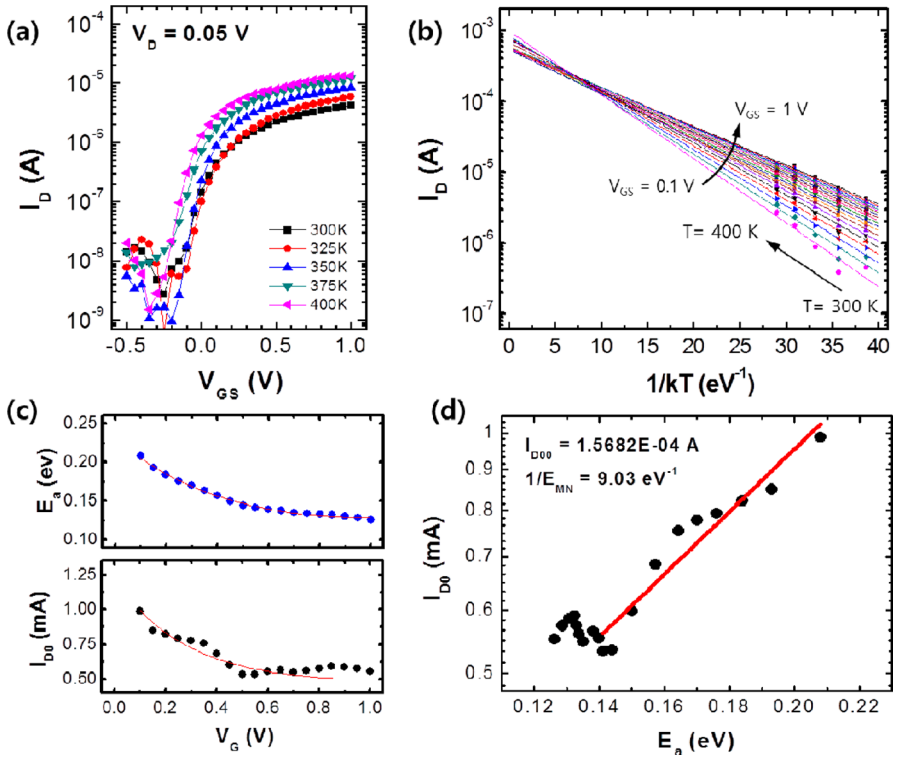

Figure 3. (a) Transfer characteristics of the MoS_2-based EDLT devices measured at various temperatures, ranging from 300 to 400 K. (b) Temperature dependence of the drain current, I_D. Scattered points represent the measured data, and the lines are fitted data to extract E_a. (c) Activation energy (E_a) and prefactor (I_{D0}) as a function of V_G. (d) I_{D0} vs E_a plot to estimate the Meyer-Neldel parameter (E_{MN}).

range from 10^{-1} Hz to 10^6 Hz. The homemade metal electrode−insulator−metal electrode (MIM) cells were configured for the measurement of the ionic conductivity and capacitance. $BMimBF_4$ ILs (used as insulating materials) were inserted into a 1 cm wide space of MIM cells between two Ti/Au electrodes with a contact area of 1 cm^2. The cell was made up of PTFE to prevent melting or unexpected side reactions at elevated temperatures. The electrical EDLT characterization was performed with a semiconductor characterization system (Keithley 4200 SCS) connected to the probe station.

3. RESULTS AND DISCUSSION

Figure 1a shows the chemical structure of $BMimBF_4$, which is the representative imidazolum family IL due to their relatively high ionic conductivity and thermal stability.[11−13] In fact, for EDLTs, the capacitive behavior and ionic transport of the IL electrolytes significantly influence the device features. Thus, we confirmed the temperature dependence of $BMimBF_4$ in the range of 300−400 K by impedance spectroscopy. As shown in Figure 1b, the ionic conductivities of ILs were enhanced at elevated temperatures due to the facilitated ion transport. The activation energy for ionic conduction, which can be derived from the Arrhenius equation, was determined to be 0.19 eV, indicating an ion hopping mechanism through acid−base pairs between protonated imidazolium rings and tetrafluoroborate anions.[14] The DC capacitances of Figure 1c in the $BMimBF_4$ ILs were calculated at different temperatures using the equation: $C = -1/2\pi f Z''$, where C is the DC capacitance, f is the frequency (in a range from 10^{-1} to 10^6 Hz), and Z″ is the imaginary impedance. The calculated capacitance value at 300 K was 3.63 $\mu F/cm^2$ (at a frequency of $\sim 10^{-1}$ Hz), which is in good agreement with previous literature[15] and is about 3 orders of magnitude greater than that of a several hundred nanometer thick SiO_2 dielectric. Importantly, the capacitance value was enhanced as a function of temperature due to the thermally activated ion transport. As a result, the DC capacitances at 400 K at the same frequency were improved up to 12.4 $\mu F/cm^2$, which is three times greater than the value at 300 K. In a similar manner, we also estimate the resistivity values at different temperatures. Even above 80 °C, typical polymer electrolytes drastically change values due to the evaporation of the conduction media (i.e., water),[16] but the resistivity of the $BMimBF_4$ ILs is still consistent due to the humidity-independent transport mechanism as shown in Figure 1d (combined with capacitance). This finding should be addressed again because the thermally stable ion transports of the ILs would ensure that the EDLT system can be properly operated at the elevated temperatures.

Figure 2a illustrates a schematic device configuration of the MoS_2 nanosheet-based EDLT with IL. As described in the Experimental Section, Ti/Au electrodes and $BMimBF_4$ were used as source/drain electrodes and dielectric, respectively. Figure 2b displays the measured transfer characteristics (source-drain current, I_{DS}, as a function of the gate voltage, V_G) of the MoS_2 EDLTs at a fixed source-drain voltage, V_{DS}, of 0.05 V. The source−drain current I_{DS} increased in proportion to the gate voltage (V_G) in the positive direction up to 1 V. This behavior of MoS_2 EDLTs corresponds to the typical characteristics of n-type transistors, where the Fermi level is deep in the conduction band. Although the slight hysteresis of MoS_2 EDLTs was observed at this scanning speed (12.5 mV/s) of gate bias, the feature of the transfer curve was consistent in both the forward and reverse scans of V_G. The threshold voltage (V_T) was −0.2 V. This low-operation voltage has the advantage of exceptionally high capacitance values for both

dx.doi.org/10.1021/jp5063836 | J. Phys. Chem. C 2014, 118, 18278−18282

EDL and the 2D-nanosheet channel. As further supported by a log-scale plot of I_{DS} near the onset of electron conduction, the subthreshold swing of 80 mV/decade for the electrons was attributed to the coupling effect of the ion gating and the 2D MoS_2 electronics, and the high quality of the MoS_2/IL interface. Two electrostatic double layers at the metal/electrolyte and semiconductor/electrolyte are rapidly constructed due to the fast ion mobility and high capacitance of the ILs. Due to the capacitive behavior of the IL gating, a sufficient carrier concentration in the MoS_2 channel is readily accumulated. The on/off current ratio is 3.36×10^3, which is greater than that of the previously reported MoS_2 EDLTs gated by ILs. The electron mobility of the MoS_2-based ELDTs in the linear regime was 13.3 $cm^2/(V\ s)$, which was estimated with the following equation:[14]

$$I_D = \mu W/LC_{EDL}(V_G - V_T)V_D \quad (1)$$

where L is the channel length of 9.2 μm, W is the channel width of 41 μm, and C_{EDL} is the capacitance of the dielectric. It should be noted that we used the capacitance value obtained from the impedance spectra at 0.1 Hz because it is assumed to be closer to static behavior than dynamic. The $I_{DS}-V_{DS}$ characteristics of the MoS_2 EDLTs with a gate voltage, V_G, in the range from −0.3 to 0.3 V are also presented in Figure 2c. The I_{DS} was linearly proportional to V_{DS} below a V_G of 0.5 V, indicating that the source and drain electrodes in the MoS_2-based EDLTs have a nearly ohmic contact property.

With the secured thermally tolerable characteristics of the ILs, we measured the temperature-dependent current flows of the MoS_2 EDLTs in order to render the spectral DOS in the band gap. In fact, the temperature-dependent experiments of the device are typically performed at cryogenic temperatures. However, for large bandgap semiconductors such as MoS_2, a Schottky barrier may be more prominent at low temperatures, resulting in increased contact resistance.[17] Thus, measurements of the temperature-dependent transport of the EDLTs above room temperature are more suitable in order to ensure precise extractions. Figure 3a shows the transfer curves with elevating temperatures from 300 to 400 K and steps of 25 K. When the temperature is raised, the intrinsic concentration of charge carriers in the channel increases, and the threshold voltage shifts to lower gate potentials than has been previously reported for conventional thin film transistors.[7] Even at the high temperature of 400 K, the MoS_2 EDLTs still were in the accumulation mode. The device characteristics, such as the transfer curve shape, the on-currents, and the on/off ratios, remained intact within the measurement range of the temperature.

Figure 3b, which shows the temperature dependent I_{DS} extracted from Figure 3a, shows the thermally activated drain currents (I_D) of the MoS_2-based EDLTs, where the currents can be described by

$$I_D = I_{D0} \exp(-E_a/kT) \quad (2)$$

where I_{D0} is the prefactor, E_a is the activation energy, k is the Boltzmann constant, and T is the temperature. In particular, I_{D0} and E_a, which are extracted from the $\log(I_D)$ vs $1/kT$ plots, can be varied with V_G as shown in Figure 3c and have a correlation known as the Meyer-Neldel (MN) rule:[18,19]

$$I_{D0} = I_{D00} \exp(E_a/E_{MN}) \quad (3)$$

and this relation leads to the following equation:

$$I_D = I_{D00} \exp[(1/E_{MN} - 1/kT)E_a] \quad (4)$$

where I_{D00} is the characteristic constant and E_{MN} is defined as the MN energy, which is the common cross point shown in Figure 3b. Figure 3d shows that $1/E_{MN}$ for our MoS_2-based EDLTs is valid at 9.03 eV^{-1} in a range of activation energies from 0.14 to 0.21 eV, and I_{D00} is ∼0.157 mA. Collectively, these MN relations in the MoS_2 EDLT device indicate that the Fermi level, E_F, is varied by V_G despite the introduction of the defect states of the MoS_2 semiconductor surfaces. Consistent with this, the energy difference between E_F of the semiconductor and the band edge at the insulator-semiconductor interface is approximated with the measured E_a (V_G) of I_D and can be expressed as $E_a = E_F - E_C - qV_i$, where V_i is the potential right at the IL contact with the MoS_2 semiconductor, which is close to zero.[20,21] As V_G increases, the induced carrier density per unit area corresponding to $n_{2D} = (C_{EDL}\Delta V_G)/q$ increasingly fills the localized states from a lower energy level. Therefore, the increased number of charge carriers induced in the MoS_2 surface decreases E_a. In consideration that the MoS_2 layers were mechanically detached from bulk MoS_2 crystals, and thus the induced charge density should be much larger than the trap sites, we can estimate the induced surface charge DOS of the MoS_2, $n_{2D}(E)$, to be

$$n_{2D}(E) = \frac{C_{EDL}}{q}\left(\frac{dE_a}{dV_G}\right)^{-1} \quad (5)$$

Figure 4 shows $n_{2D}(E)$ and n_{2D} for a 5×5 MoS_2 supercell as a function of the corresponding energy level.[22] An abrupt

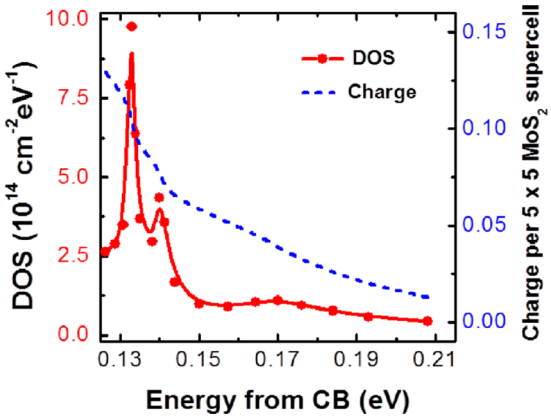

Figure 4. Surface charge density of states of the MoS_2 in the EDLT devices and total charge concentration per 5×5 MoS_2 supercell corresponding to the energy level from the conduction band.

decrease is observed in the n_{2D} values to ∼0.14 eV below the conduction bands, and the monotonous reduction of the values from the crossed level of the two distinct n_{2D} function lines. This relatively short band edge region can also be the reason for the near-ideal subthreshold swings of the MoS_2 EDLT devices. On the other hand, in contrast to the traces of n_{2D}, there are some peaks that individually represent their energy states with respect to the surface DOS (cm^{-2} eV^{-1}). The most interesting peaks are measured at 0.135 and 0.145 eV below the conduction band, with the largest DOS values of 9.75×10^{14} and 4.33×10^{14} cm^{-2} eV^{-1}, respectively. At the moment, the origin of these distinct peaks is unclear, but if we pay attention to the fact that the bandgap of the MoS_2 nanosheet strongly depends on the number of MoS_2 layers, a possible explanation

dx.doi.org/10.1021/jp5063836 | J. Phys. Chem. C 2014, 118, 18278−18282

may be the fact that the monolayer MoS_2 nanosheets coexist with the MoS_2 multilayer in the channel area of the EDLT.[23]

4. CONCLUSION

In conclusion, we have fabricated high-performance MoS_2-based EDLT devices with high thermal stability, which allow for the performance of the variable temperature measurements on MoS_2-based EDLT. Observed temperature-dependent behavior of activation energy for electron transport confirmed that the MN rule can be applied to the charge transport in the MoS_2 layer under high charge density. Furthermore, the 2D DOS profiles in the MoS_2 nanosheets were rigorously calculated by the stable measurements on the temperature-dependent I−V characteristics. The extracted surface DOS of the MoS_2 nanolayer shows two featured peaks at 0.135 and 0.145 eV below the conduction band, which suggest that the different energy levels are overlaid in the sub-bandgap, owing to the coexistence of monolayer and multilayers in the MoS_2 nanocrystals.

AUTHOR INFORMATION

Corresponding Authors

*E-mail: seonkuk@khu.ac.kr.

*E-mail: milleniumphs@gmail.com.

Author Contributions

‖Y.L. and J.L. contributed equally to this work.

Notes

The authors declare no competing financial interest.

ACKNOWLEDGMENTS

This research was also supported by the National Research Foundation of Korea (NRF-2013K1A3A1A32035549, NRF-2012R1A1A1042630, and NRF-2013-220-2013S1A2A2035510) and a grant from the Fundamental R&D Program for Core Technology of Materials funded by the Ministry of Trade, Industry & Energy.

REFERENCES

(1) Novoselov, K. S.; Jiang, D.; Schedin, F.; Booth, T. J.; Khotkevich, V. V.; Morozov, S. V.; Geim, A. K. Two-dimensional atomic crystals. *Proc. Natl. Acad. Sci. U.S.A* **2005**, *102*, 10451−10453.

(2) Bolotin, K. I.; Sikes, K. J.; Jiang, Z.; Klima, M.; Fudenberg, G.; Hone, J.; Kim, P.; Stormer, H. L. Ultrahigh electron mobility in suspended graphene. *Solid State Commun.* **2008**, *146*, 351−355.

(3) Ponomarenko, L. A.; Schedin, F.; Katsnelson, M. I.; Yang, R.; Hill, E. W.; Novoselov, K. S.; Geim, A. K. Chaotic dirac billiard in graphene quantum dots. *Science* **2008**, *320*, 356−358.

(4) Kim, K. S.; Zhao, Y.; Jang, H.; Lee, S. Y.; Kim, J. M.; Kim, K. S.; Ahn, J.-H.; Kim, P.; Choi, J.-Y.; Hong, B. H. Large-scale pattern growth of graphene films for stretchable transparent electrodes. *Nature* **2009**, *457*, 706−710.

(5) Kim, B. J.; Jang, H.; Lee, S.-K.; Hong, B. H.; Ahn, J.-H.; Cho, J. H. High-performance flexible graphene field effect transistors with ion gel gate dielectrics. *Nano Lett.* **2010**, *10*, 3464−3466.

(6) Radisavljevic, B.; Radenovic, A.; Brivio, J.; Giacometti, V.; Kis, A. Single-layer MoS_2 transistors. *Nat. Nanotechnol.* **2011**, *6*, 147−150.

(7) Kim, S.; Konar, A.; Hwang, W.-S.; Lee, J. H.; Lee, J.; Yang, J.; Jung, C.; Kim, H.; Yoo, J.-B.; Choi, J.-Y.; et al. High-mobility and low-power thin-film transistors based on multilayer MoS_2 crystals. *Nat. Commun.* **2012**, *3*, 1011.

(8) Perera, M. M.; Lin, M.-W.; Chuang, H.-J.; Chamlagain, B. P.; Wang, C.; Tan, X.; Cheng, M. M.-C.; Tománek, D.; Zhou, Z. Improved carrier mobility in few-layer MoS_2 field-effect transistors with ionic-liquid gating. *ACS Nano* **2013**, *7*, 4449−4458.

(9) Ozel, T.; Gaur, A.; Rogers, J. A.; Shim, M. Polymer electrolyte gating of carbon nanotube network transistors. *Nano Lett.* **2005**, *5*, 905−911.

(10) Lee, J.; Panzer, M. J.; He, Y.; Lodge, T. P.; Frisbie, C. D. Ion gel gated polymer thin-film transistors. *J. Am. Chem. Soc.* **2007**, *129*, 4532−4533.

(11) Dupont, J.; de Souza, R. F.; Suarez, P. A. Z. Ionic liquid (molten salt) phase organometallic catalysis. *Chem. Rev.* **2002**, *102*, 3667−3692.

(12) Buzzeo, M. C.; Evans, R. G.; Compton, R. G. Non-haloaluminate room-temperature ionic liquids in electrochemistry: A review. *ChemPhysChem* **2004**, *5*, 1106−1120.

(13) Blanchard, L. A.; Hancu, D.; Beckman, E. J.; Brennecke, J. F. Green processing using ionic liquids and CO_2. *Nature* **1999**, *399*, 28−29.

(14) Park, H. S.; Choi, Y. S.; Kim, Y. J.; Hong, W. H.; Song, H. 1D and 3D Ionic liquid−aluminum hydroxide hybrids prepared via an ionothermal process. *Adv. Funct. Mater.* **2007**, *17*, 2411−2418.

(15) Hu, Z.; Vatamanu, J.; Borodin, O.; Bedrov, D. A molecular dynamics simulation study of the electric double layer and capacitance of [BMIM][PF_6] and [BMIM][BF_4] room temperature ionic liquids near charged surfaces. *Phys. Chem. Chem. Phys.* **2013**, *15*, 14234−14247.

(16) Choi, B. G.; Hong, J.; Park, Y. C.; Jung, D. H.; Hong, W. H.; Hammond, P. T.; Park, H. Innovative polymer nanocomposite electrolytes: Nanoscale manipulation of ion channels by functionalized graphenes. *ACS Nano* **2011**, *5*, 5167−5174.

(17) Sze, S. M. *Physics of semiconductor devices*, 2nd ed.; John Wiley & Sons, Inc.: New York, 1981.

(18) Meyer, W.; Neldel, H. Relation between the energy constant and the quantity constant in the conductivity−temperature formula of oxide semiconductors. *Z. Technol. Phys.* **1937**, *12*, 588−593.

(19) Chen, C.; Abe, K.; Kumomi, H.; Kanicki, J. Density of states of a-InGaZnO from temperature-dependent field-effect studies. *IEEE Trans. Electron Devices* **2009**, *56*, 1177−1183.

(20) Lang, D. V.; Chi, X.; Siegrist, T.; Sergent, A. M.; Ramirez, A. P. Amorphouslike density of gap states in single-crystal pentacene. *Phys. Rev. Lett.* **2004**, *93*, 086802.

(21) Kalb, W. L.; Batlogg, B. Calculating the trap density of states in organic field-effect transistors from experiment: A comparison of different methods. *Phys. Rev. B* **2010**, *81*, 035327.

(22) Dolui, K.; Rungger, I.; Pemmaraju, C. D.; Sanvito, S. Possible doping strategies for MoS_2 monolayers: An ab initio study. *Phys. Rev. B* **2013**, *88*, 075420.

(23) Choi, W.; Cho, M. Y.; Konar, A.; Lee, J. H.; Cha, G. B.; Hong, S. C.; Kim, S.; Kim, J.; Jena, D.; Joo, J. High-detectivity multilayer MoS_2 phototransistors with spectral response from ultraviolet to infrared. *Adv. Mater.* **2012**, *24*, 5832−5836.